

Navigation of *C. elegans* in three-dimensional media: roll maneuvers and planar turns

Alejandro Bilbao,¹ Amar K. Patel,¹ Mizanur Rahman,² Siva A. Vanapalli,² and Jerzy Blawdziewicz³

¹*Department of Mechanical Engineering, Texas Tech University, Lubbock, Texas, U.S.A.*

²*Department of Chemical Engineering, Texas Tech University, Lubbock, Texas, U.S.A.*

³*Departments of Mechanical Engineering and Physics, Texas Tech University, Lubbock, Texas, U.S.A.*

Free-living nematode *Caenorhabditis elegans* is a powerful genetic model, essential for investigations ranging from behavior to neuroscience to aging, and locomotion is a key observable used in these studies. However, despite the fact that in its natural environment *C. elegans* moves in three-dimensional (3D) complex media (decomposing organic matter and water), quantitative investigations of its locomotion have been limited to two-dimensional (2D) motion. Based on our recent quantitative analysis of 2D turning maneuvers [Phys. Fluids 25, 081902 (2013)] we follow with the first quantitative description of how *C. elegans* moves in 3D environments. We show that by superposing body torsion and 2D undulations, a burrowing or swimming nematode can rotate the undulation plane. A combination of these roll maneuvers and 2D turns associated with variation of undulation-wave parameters allows the nematode to explore 3D space. We apply our model to analyze 3D chemotaxis of nematodes burrowing in a gel and swimming in water; we conclude that the nematode can achieve efficient chemotaxis in different environments without adjusting its sensory-motor response to chemical signals. Implications of our findings for understanding of 3D neuromuscular control of nematode body are discussed.

Keywords: *Caenorhabditis elegans*, locomotion, hydrodynamic bead models, chemotaxis, neuromuscular control, 3D environment

1. INTRODUCTION

Investigations of locomotion of a free-living nematode *C. elegans* (one of the most important model organisms) can reveal a wealth of information on physiology, muscle biology, and neural control of movement and behavior. Efficient locomotion depends on muscular strength [1–3], neuromuscular coordination [4, 5], and information processing [6, 7]. Locomotory readouts are thus extensively used to describe impacts of genetic mutations [8–10] and evaluate pharmacological effects [11, 12].

In its natural environment (soil rich in decaying organic matter), *C. elegans* interacts with a complex three-dimensional (3D) surrounding medium that includes rainwater and soft organic materials. Most studies of nematode locomotion, however, have focused on two-dimensional (2D) motion [13–17], and little effort has been made to characterize worm motility in 3D environments that would mimic *C. elegans* natural habitat.

Only recently was 3D burrowing motion of *C. elegans* in soft substrates quantitatively imaged [18] and feasibility of using 3D motion to assess genetic mutations [19] and to identify muscular dystrophy [20] experimentally demonstrated. Such 3D methods of scoring *C. elegans* locomotory behavior are promising; however, unleashing the full potential of such techniques requires complementary modeling efforts to elucidate the biomechanics and neuromuscular control of 3D locomotion.

Very few quantitative analyses of 3D locomotion of *C. elegans* have been reported [21, 22]; no investigations present a realistic mathematical description of nematode motion. Our study aims to fill this knowledge gap by providing quantitative understanding of the geometry and

mechanics of 3D maneuvers of *C. elegans* burrowing in gel-like materials and swimming in Newtonian fluids.

Our modeling approach generalizes the recently proposed piecewise harmonic curvature (PHC) model of 2D nematode gait [16]. The PHC model has been shown to give an accurate parameterization of body postures (defined by the configuration of the body centerline [17, 23–25]) and of entire trails of nematodes crawling on agar without sidewise slip; it also yields a convenient quantification of time-lapse sequences of body postures in swimming.

In the present paper we expand the PHC gait model by including curve torsion in the description of the nematode postures. We show that combining the PHC model for the line curvature with a piecewise constant torsion (PCT) assumption, we can generate three-dimensional trajectories that mimic paths of burrowing nematodes. Using, in addition, our hydrodynamic models of swimming dynamics [26], we can describe 3D motion of *C. elegans* in bulk fluids. In particular, our gait model reproduces the rapid undulation-plane reorientation observed in our experiments.

The explicit PHC representation of the nematode gait has been shown to be a useful tool for quantitative investigations of swimming efficiency and 2D turning maneuvers [26]. The combined PHC/PCT gait model will help analyze diverse aspects of 3D undulatory locomotion of *C. elegans* in complex media, including chemotaxis and mechanisms of neuro-muscular actuation of body movements. To illustrate the former application we present an analysis of the efficiency of 3D chemotaxis of burrowing and swimming *C. elegans*.

Our paper is organized as follows. In Sec. 2 we develop geometrical gait models for *C. elegans* moving in

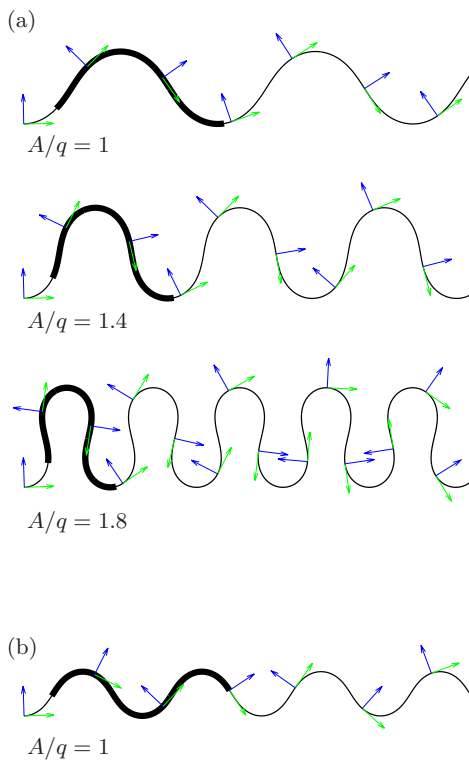


FIG. 1. (Colour online) Family of curves reproduced from harmonic curvature (3) for normalized amplitude A/q as labeled. The green and blue arrows are the unit tangent and normal vectors, respectively. The body of a nematode moving along the curves is represented by the thick line segments of length L . Two normalized wavevectors are shown (a) $qL = 5.5$ (typical swimming gait) and (b) $qL = 9$ (typical crawling gait). Depending on the wavevector, the normalized amplitude $A/q = 1$ may correspond to (a) C -shaped (top) and (b) W -shaped body postures; $A/q = 1.8$ produces an Ω -shaped body posture.

2D and 3D. We also assess the effectiveness of reorientation maneuvers of animals crawling on a flat 2D substrate and burrowing in soft 3D matter. In Sec. 3 we present our hydrodynamic analysis of reorientation maneuvers of *C. elegans* swimming in a viscous fluid. The geometrical and hydrodynamic locomotion descriptions developed in Secs. 2 and 3 are combined in Sec. 4 with simple models of chemosensation and motion control to describe chemotaxis of burrowing and swimming *C. elegans* in 3D. Implications of our findings for the emerging area of 3D undulatory locomotion are discussed in Sec. 5.

2. GEOMETRICAL DESCRIPTION OF THE NEMATODE GAIT

Caenorhabditis elegans crawling on or burrowing through a soft gel-like substrate (such as agar) often move with no transverse slip with respect to the environment.

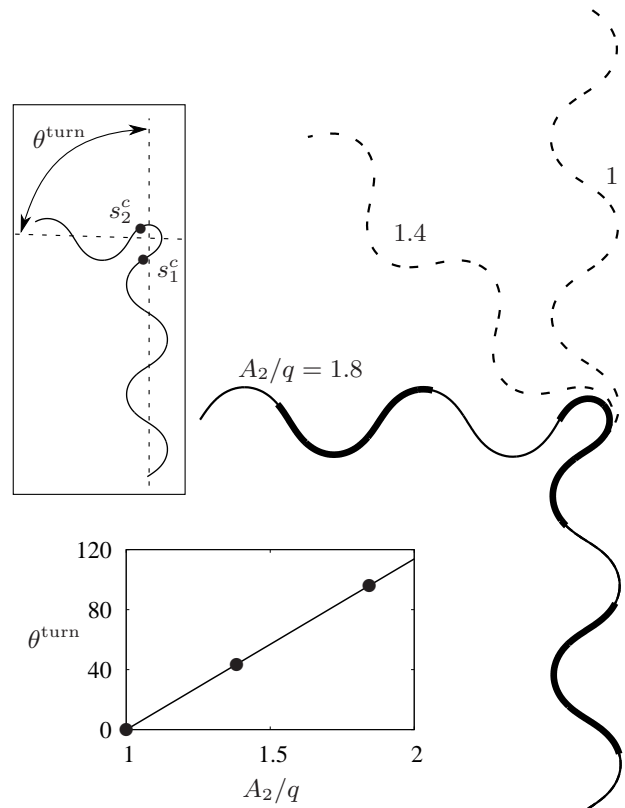


FIG. 2. A crawling nematode performing three-mode planar turn with the default-mode amplitude $A_1/q = 1$ and turning-mode amplitude A_2/q as labeled, for $qs_1^c = 3\pi/2$ and $q\Delta s^c = 0.6$. The turn angle θ^{turn} and mode-switching points s_1^c and s_2^c are defined in the top inset. Bottom inset shows the dependence of the turn angle θ^{turn} (in degrees) on the turning-mode amplitude A_2/q . The black dots correspond to the amplitudes of the trajectories shown.

On a moist porous surface, slip may be hindered by interfacial forces associated with water meniscus surrounding the nematode body; in a 3D gel-like medium, transverse displacements are prevented by a nonzero yield stress.

In the absence of transverse slip, all segments of the nematode body follow a single trail, which is completely determined by the geometry of the crawling or burrowing gait. Thus, for a given sequence of nematode movements, the trajectory does not depend on the substrate mechanics. Here we focus on this purely geometrical no-slip case.

In Sec. 2.1 we summarize our previously reported PHC model [16] for describing body postures and trajectories of *C. elegans* moving in two dimensions. In Sec. 2.2 we expand our model by adding a torsion component to the 2D gait representation to achieve a 3D generalization of the previously established PHC approach.

Based on our earlier analyses of *C. elegans* swimming in two dimensions [16, 26], we assume that PHC model and its 3D generalization provide a realistic representation for the swimming gait. In Sec. 3 the results derived in Sec. 2 are used to develop a comprehensive analysis that combines the gait geometry and motion mechanics

to fully describe 3D maneuvers of swimming *C. elegans*.

2.1. Description in 2D

The body of *C. elegans* is highly elongated, and therefore its postures can be faithfully represented by the body centerline [16, 17, 27]. In our analysis, the shape of the centerline is described by the worm curvature function $\kappa_w(s', t)$, where t denotes time and s' is the arclength coordinate along the body. In what follows $s' = 0$ is the tail and $s' = L$ is the head coordinate value (where L is the nematode length). The body configuration is fully determined by providing the curvature function κ_w and the position and orientation of the nematode head (or any other reference point along the body).

A curvilinear trail followed by the body of a nematode crawling with no transverse slip can be described using the trail curvature $\kappa(s)$, where s is the arclength coordinate along the trail. Since at any given time t the configuration of the nematode body coincides with a trail segment (see Fig. 1), the worm and trail curvature functions are related

$$\kappa_w(s', t) = \kappa(s' + v_s t), \quad (1)$$

where v_s is the velocity along the trail. Body postures and the trail followed by a nematode are constructed from the curvature (1) by solving the Serret–Frenet equations [28]

$$\frac{d\hat{t}}{ds} = \kappa\hat{n}, \quad (2a)$$

$$\frac{d\hat{n}}{ds} = -\kappa\hat{t}, \quad (2b)$$

where \hat{t} and \hat{n} are mutually perpendicular unit tangent and normal vectors.

Observations of *C. elegans* swimming in water indicate that the propagating-curvature-wave relation (1) applies not only to no-slip motion [in which case Eq. (1) results from geometrical constraints], but is also preserved with good accuracy when significant transverse slip occurs [16]. This behavior is a signature of the proprioceptive coupling [4] that allows the nematode to maintain a well organized gait in environments with diverse mechanical properties. Based on the similarity between the curvature wave form for crawling and swimming nematodes we formulate a unified gait description for different media.

2.1.1. PHC representation of nematode gait

Caenorhabditis elegans produces a variety of body postures, ranging from shallow undulations to highly curved Ω shapes and loop shapes. Recently, we have demonstrated [16] that all these body shapes can be accurately

represented using the harmonic curvature function

$$\kappa(s) = A \cos(qs + \phi), \quad (3)$$

where A is the wave amplitude, $q = 2\pi/\lambda$ is the wavevector (with λ denoting the wavelength), and ϕ is the phase angle.

Combining Eqs. (1)–(3) yields a family of curves representative of the most common nematode postures. For moderate values of the dimensionless amplitude $A/q \approx 1$, typical crawling postures (W -shaped) and swimming postures (C -shaped) are obtained, as illustrated in Fig. 1. Higher amplitudes correspond to Ω -shapes ($A/q \approx 2$) and loop shapes ($A/q \approx 3$, described in [16]).

According to the PHC model [16], trails of crawling nematodes can be accurately represented by the harmonic function (3) with abruptly changing wave parameters A , q , and ϕ between harmonic-curvature intervals. Such changes generate either small fluctuations in the direction of motion or significant body reorientation, depending on the magnitude of the parameter variation and the mode switching point.

2.1.2. Planar turns

To investigate the turning ability of *C. elegans*, we consider three-mode PHC maneuvers. More complex trajectories can be obtained by combining three-mode turns. For simplicity, we focus on maneuvers in which only the amplitude of the harmonic curvature varies,

$$\kappa(s) = \begin{cases} A_1 \cos(qs), & s < s_1^c, \\ A_2 \cos(qs), & s_1^c < s < s_2^c, \\ A_1 \cos(qs), & s_2^c < s, \end{cases} \quad (4)$$

where A_1 is the base crawling amplitude (with $A_1/q \approx 1$), $A_2 > A_1$ is the turning amplitude, and s_1^c and s_2^c are the mode-switching points. Planar turns can also be obtained by tuning the wavevector and phase angle; an analysis of such turns is presented in the Electronic Supplementary Material (ESM).

Figure 2 shows an example of a crawling nematode executing a three-mode planar turn for fixed switching points s_1^c and s_2^c and several values of the normalized turning mode amplitudes A_2/q . The dependence of the turn angle θ^{turn} (defined in the top inset of Fig. 2) on the turn amplitude A_2 is depicted in the bottom inset of Fig. 2.

2.2. Description in 3D

Caenorhabditis elegans, which crawls and burrows in rotting vegetation and swims in rainwater, performs 2D and 3D maneuvers [18, 29, 30] to find optimal environmental conditions. Existing literature focuses nearly exclusively on 2D motion, and 3D models of nematode gait

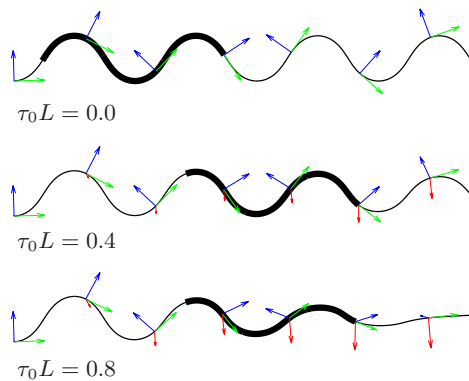


FIG. 3. (Colour online). Curves defined by the harmonic curvature (normalized amplitude $A/q = 1$) and constant torsion (normalized magnitude $\tau_0 L$ as labeled); worm contours (thick line segments) correspond to $qL = 9$. The green, blue and red arrows are the unit tangent, normal, and binormal vectors, respectively.

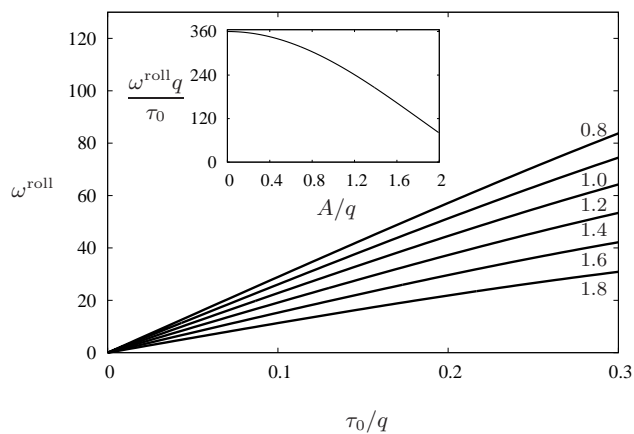


FIG. 4. Roll rotation rate per undulation period ω^{roll} (in degrees) vs normalized body torsion τ_0/q for one-mode torsional roll with harmonic-curvature amplitude A/q as labeled. Inset shows the dependence of the line slope $\omega^{\text{roll}}/q/\tau_0$ on the amplitude A/q .

and locomotion mechanics are unavailable. In this section we expand our PHC model to incorporate 3D nematode postures and trails into the gait representation.

The proposed description is motivated by recent observations of 3D body postures in crawling [21], burrowing [18], and swimming. A crawling *C. elegans*, for example, can produce torsional deformation of its body, resulting in detachment of some body sections from the underlying surface, as shown in the images of crawling worms in Ref. [21]. Swimming nematodes undergo a similar out-of-plane body deformations, accompanied by rapid rotation of the undulation plane (see Sec. 3). Three-dimensional body actuation seems also to occur for nictating nematodes (see supplemental movies in [31]).

To incorporate out-of-plane body postures into the PHC model, we use the complete 3D set of Serret–Frenet

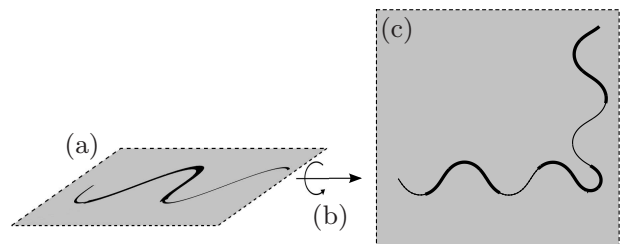


FIG. 5. Nematode reorientation in 3D. The nematode (a) undulates in the initial plane of motion; (b) executes a torsional roll maneuver; and (c) performs planar turn in the new plane of motion.

equations,

$$\frac{d\hat{\mathbf{t}}}{ds} = \kappa\hat{\mathbf{n}}, \quad (5a)$$

$$\frac{d\hat{\mathbf{n}}}{ds} = -\kappa\hat{\mathbf{t}} + \tau\hat{\mathbf{b}}, \quad (5b)$$

$$\frac{d\hat{\mathbf{b}}}{ds} = -\tau\hat{\mathbf{n}}, \quad (5c)$$

which includes both the curvature and torsion components. Here $\tau = \tau(s)$ is the torsion of the curve defining the 3D nematode trail, $\hat{\mathbf{t}}$ is the tangent unit vector, $\hat{\mathbf{n}}$ is the normal unit vector in the local undulation plane, and $\hat{\mathbf{b}} = \hat{\mathbf{t}} \times \hat{\mathbf{n}}$ is the binormal unit vector (normal to the local undulation plane). The curve torsion τ , which corresponds to the rotation of the Serret–Frenet basis $(\hat{\mathbf{t}}, \hat{\mathbf{n}}, \hat{\mathbf{b}})$ about the tangent direction $\hat{\mathbf{t}}$, results in out-of-plane deformations of the curve.

2.2.1. Constant-torsion assumption

Quantitative experimental information regarding out-of-plane body postures of *C. elegans* is very limited. However, a qualitative examination of nematode images suggests that key features of 3D nematode gait can be reproduced by combining the harmonic curvature model (3) with the constant-torsion assumption,

$$\tau(s) = \tau_0. \quad (6)$$

The solution of the Serret–Frenet equations (5) with the curvature and torsion given by equations (3) and (6) is depicted in Fig. 3. The results indicate that the general shape of the body wave is preserved in the presence of nonzero torsion, but the undulation plane rotates with the angular velocity proportional to the torsion amplitude τ_0 . This behavior is in a qualitative agreement with the crawling nematode image shown in Ref. [21]. The gait described by Eqs. (3) and (6) will be called a single-mode torsional roll.

Figure 4 shows the torsional-roll rotation rate per undulation period,

$$\omega^{\text{roll}} = \cos^{-1} \left[\hat{\mathbf{b}}(0) \cdot \hat{\mathbf{b}}(2\pi/q) \right]. \quad (7)$$

The rotation rate (7) is determined from the angle between the binormal vectors at $s = 0$ and $s = 2\pi/q$; it depends linearly on the dimensionless torsion τ_0/q . According to the results in Fig. 4, the slope of the lines ω^{roll} vs τ_0/q decreases with the increasing dimensionless curvature-wave amplitude A/q . The decrease stems from the fact that only the projection of the torsion vector $\boldsymbol{\tau} = \tau\hat{\mathbf{t}}$ onto the average direction of motion contributes to the roll.

2.2.2. Three-mode roll maneuvers

In the case of variable torsion, we assume that the torsion wave $\tau_w(s', t)$ propagates backward along the nematode body,

$$\tau_w(s', t) = \tau(s' + v_s t), \quad (8)$$

similar to the curvature wave (1). For no-slip motion (e.g., burrowing in a gel), relation (8) is required by the constraints that all segments of the nematode body follow a single trail. By analogy with our 2D results [16], we assume that the form (8) also applies to swimming.

According to our qualitative observations of nematode motion in water, *C. elegans* survey their environment producing roll reorientation maneuvers at irregular intervals. To replicate such motions in burrowing and swimming, we introduce a three-mode roll, where the nematode performs one-mode harmonic curvature undulations (1) superposed with piecewise constant torsion

$$\tau(s) = \begin{cases} 0, & s < s_1^\tau, \\ \tau_0, & s_1^\tau < s < s_2^\tau, \\ 0, & s_2^\tau < s, \end{cases} \quad (9)$$

(where s_1^τ and s_2^τ are the mode switching points, and $\Delta s^\tau = s_2^\tau - s_1^\tau$ is the roll-mode length). By combining torsional roll maneuvers with three-mode planar turns, a nematode is capable of exploring 3D space (see Fig. 5 and Video S1 in ESM).

3. NEMATODE MANEUVERABILITY IN FLUIDS

The PHC and PHC/PCT gait representations developed in Sec. 2 will now be combined with a hydrodynamic bead-based model to describe body reorienting maneuvers performed by swimming *C. elegans*. To account for hydrodynamic forces, the nematode body is approximated by an active chain of hydrodynamically coupled spheres arranged along the body centerline described by Eqs. (4) and (9) (see simulation images shown in Fig. 6).

The hydrodynamic forces and torques acting on the chain are calculated in the Stokes-flow limit using the generalized Rotne-Prager approximation [32]. This approximation is much faster (although less accurate) than

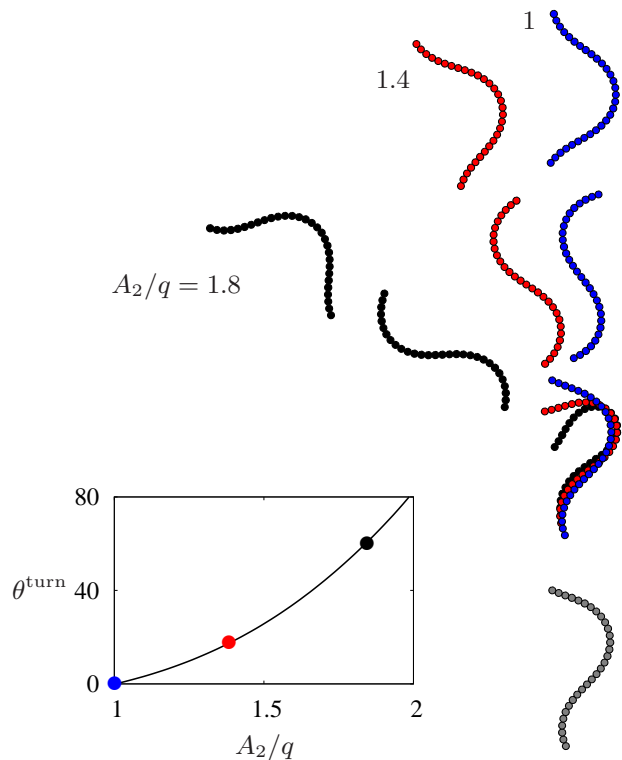


FIG. 6. (Colour online) A sequence of snapshots of a swimming *C*-shaped nematode ($qL = 5.5$) performing a three-mode planar turn with the default-mode amplitude $A_1/q = 1$ and turning mode amplitude as labeled, for $qs_1^c = 3\pi/2$ and $q\Delta s^c = 0.6$. The gray image represents the starting position for all trajectories. The inset shows the dependence of the turn angle θ^{turn} (in degrees) on the turning-mode amplitude A_2/q . The dots correspond to the snapshots shown.

the HYDROMULTIPOLE algorithm [33] used in our previous study [26].

Our methods for calculating the hydrodynamic friction and mobility tensors are described in Ref. [26] and in ESM. We note that in an independent study Berman *et al.* [25] also used a hydrodynamic bead-based model to investigate undulatory swimming of a nematode.

3.1. Swimming in 2D

To assess 2D reorientation ability of swimming *C. elegans*, we consider trajectories of a nematode performing three-mode PHC turns, and evaluate the angle θ^{turn} between the initial and final swimming directions. Similar to our analysis of no-slip turns (Sec. 2.1.2), the nematode initially swims using the default forward-locomotion mode with the amplitude $A/q = 1$, switches to a higher-amplitude turning mode, and returns to the default mode. Due to hydrodynamic effects, the turn angle in swimming depends not only on the curvature-wave and torsion-wave parameters, but also on the nematode length L .

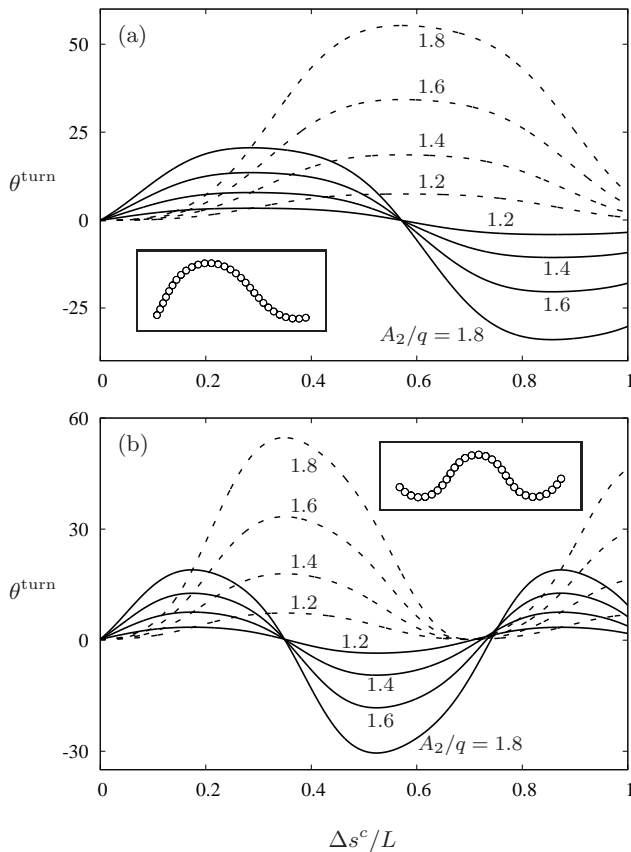


FIG. 7. Planar turn angle θ^{turn} (in degrees) vs normalized turning-mode length $\Delta s^c/L$ for (a) *C*-shaped ($qL = 5.5$) and (b) *W*-shaped ($qL = 9$) nematodes (see insets) and turning-mode amplitude A_2/q as labeled. Turns initiated at $qs_1^c = 0$ (solid lines) and $\frac{3}{2}\pi$ (dashed). The normalized amplitude of the default forward mode is $A_1/q = 1$.

A comparison of the numerical simulations depicted in Fig. 6 with the corresponding results for a nematode crawling without sidewise slip (Fig. 2) indicates that a swimming nematode produces shallower turns than its crawling counterpart. Moreover, due to the nonlinear dependence of the hydrodynamic interactions on the body posture, in swimming the relation between the turn angle θ^{turn} and the amplitude of the turning mode A_2/q is nonlinear (in contrast to the linear dependence for no-slip motion).

Figure 7 provides further details regarding the dependence of the turn angle θ^{turn} on the turning-mode parameters. The results, for different values of the turning mode amplitude, are shown vs turning-mode length $\Delta s^c/L$ for two wavevector values: $qL = 5.5$ and $qL = 9$ (i.e., for *C*-shaped and *W*-shaped gaits). In the scaling used in Fig. 7, i.e., with the mode length Δs^c normalized by the worm length L , the results differ significantly between the two values of qL . We note, however, that the dependence of the turn angle on the gait parameter qL is much weaker when the s coordinate is normalized by the wavevector q [26], which indicates that the nematode



FIG. 8. Time-lapse images of a swimming *C. elegans* switching the plane of undulations.

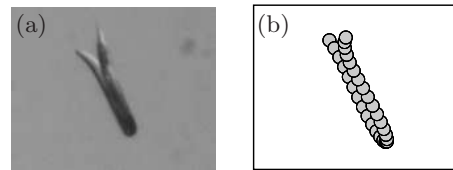


FIG. 9. (a) Non-planar body posture of a swimming *C. elegans* and (b) qualitatively matching calculated body shape with constant torsion $\tau_0 L = 0.9$ and harmonic curvature of the normalized amplitude $A/q = 1$ and wavevector $qL = 5.5$.

length has only a moderate effect on the turn dynamics.

According to the results shown in Figs. 6 and 7, a swimming nematode can control the turn angle by varying the turning-mode amplitude A as well as the turn initiation point s_1^c and turning-mode length Δs^c . Similar to the crawling case, a swimming nematode can fully explore 2D space by performing a sequence of elementary turns. For a qualitative comparison of a 2D multi-mode turn of a swimming wild-type nematode with a corresponding numerical simulation using the PHC model see video S2 in ESM.

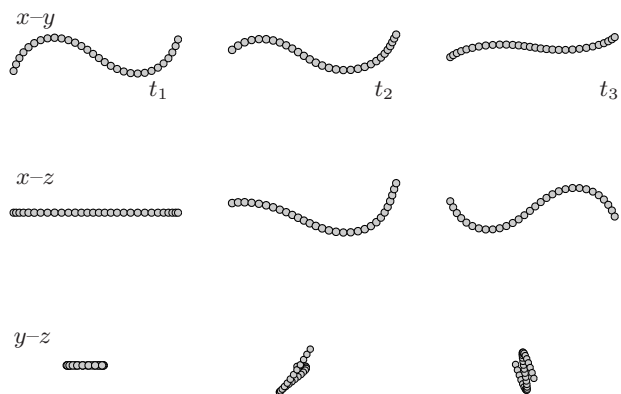


FIG. 10. Stereoscopic views of a *C*-shaped nematode ($qL = 5.5$, $A/q = 1$) performing a three-mode swimming roll maneuver (projection planes as labeled). At times t_1 and t_3 the nematode performs planar undulations; at t_2 it performs a roll with normalized torsion $\tau_0 L = 1.5$ and length $q\Delta s^c = 3.24$. The roll results in a change of the undulation plane by more than 90° .

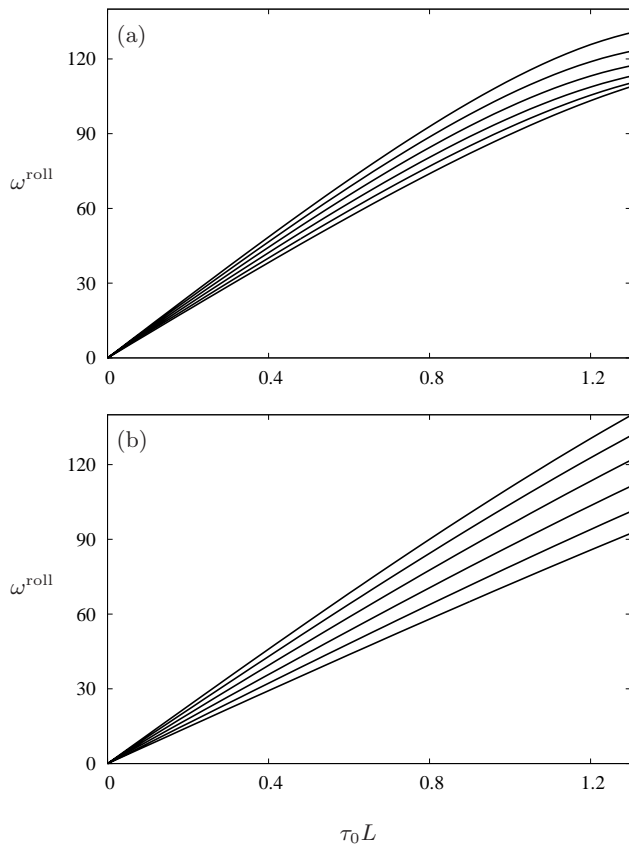


FIG. 11. Roll rotation rate per undulation period ω^{roll} (in degrees) vs normalized body torsion $\tau_0 L$, for normalized curvature-wave amplitude $A/q = 0.8, 1, 1.2, 1.4, 1.6, 1.8$ (from above) for (a) *C*-shaped ($qL = 5.5$) and (b) *W*-shaped ($qL = 9$) swimming nematodes.

3.2. Swimming in 3D

Observations of *C. elegans* swimming in bulk fluids show that the animal is able to actively explore 3D environments. A swimming nematode can perform a series of planar turns and is also capable of rapidly changing the plane of undulations (see Fig. 8 and Video S3 in ESM).

Video images of *C. elegans* undergoing undulation-plane reorientation indicate that during such maneuvers the nematode body postures are distorted out of the undulation plane. We find that these nonplanar postures resemble the torsional-roll contours defined by curvature and torsion relations (3) and (6) (see the contours depicted in Fig. 3).

Figure 9 shows a direct comparison between a video image of a swimming nematode and a calculated torsional-roll posture with a curvature wavevector $qL = 5.5$ (*C*-shaped gait) and constant torsion $\tau_0 L = 0.9$. We note that the out-of-plane deformation of the nematode body is quite small for this torsion value; our hydrodynamic analysis shows, however, that even a moderate torsional deformation may have a significant dynamic effect, producing rolls that are significantly stronger than the cor-

responding rolls in no-slip burrowing.

To elucidate the effect of the torsional roll in swimming, we present results of our hydrodynamic simulations for single-mode and three-mode roll maneuvers, described by Eq. (6) and (9), respectively. The overall undulation-plane rotation rate for a swimming nematode includes geometrical and hydrodynamic contributions. The geometrical component results from the rotation of the Serret–Frenet frame $(\hat{\mathbf{t}}, \hat{\mathbf{n}}, \hat{\mathbf{b}})$ according to equations (5); the hydrodynamic component is associated with the rigid-body rotation of the whole nematode body, as required by the zero net hydrodynamic force and torque conditions.

Figure 10 shows stereoscopic snapshots of the nematode configuration at the beginning, during, and at the end of a simulated three-mode roll. Another example of a three-mode roll maneuver is presented in Video S4 in ESM. In both cases the nematode undergoes a roll rotation of approximately 90° . Simulated nematode motion in the Video S4 closely resembles the behavior of a wild-type nematode seen in Video S3.

Quantitative results regarding the effectiveness of roll reorientation maneuvers in fluids are presented in Figs. 11–13. The roll rotation rate per undulation period (7) during a single-mode roll is plotted in Fig. 11, and the total roll reorientation angle

$$\theta^{\text{roll}} = \cos^{-1} \left[\hat{\mathbf{b}}(s_1^\tau) \cdot \hat{\mathbf{b}}(s_2^\tau) \right] \quad (10)$$

for a nematode performing a three-mode roll is plotted in Fig. 12.

The roll rotation rate ω^{roll} depicted in Fig. 11 is shown vs the dimensionless torsion amplitude $\tau_0 L$, for several values of the normalized curvature amplitude A/q , for *C*-shaped and *W*-shaped gaits. Note that in swimming the roll rotation rate depends on the nematode length whereas in no-slip burrowing ω^{roll} depends only on the torsion and curvature-wave parameters. Hence a different normalization is used in Figs. 11 (swimming) and 4 (burrowing).

In swimming, similar to the results for the no-slip roll (Fig. 4), the roll rotation rate is an increasing function of the normalized curvature-wave amplitude A/q and body torsion $\tau_0 L$, but the dependence on the torsion is nonlinear due to hydrodynamic effects. The results for *C*-shaped and *W*-shaped gaits have a similar magnitude for given values of A/q and $\tau_0 L$.

The total reorientation angle θ^{roll} during a three-mode roll maneuver is plotted in Fig. 12 vs the dimensionless torsional mode length $q\Delta s^\tau$, normalized by the wavevector of the curvature undulations. The results are similar for the *C*-shaped and *W*-shaped gaits and are only moderately affected by the initial mode switching point. The magnitude of the reorientation angle θ^{roll} is consistent with the single-mode roll rotation rate presented in Fig. 11.

Our experimental observations of *C. elegans* swimming maneuvers indicate that the nematode typically needs

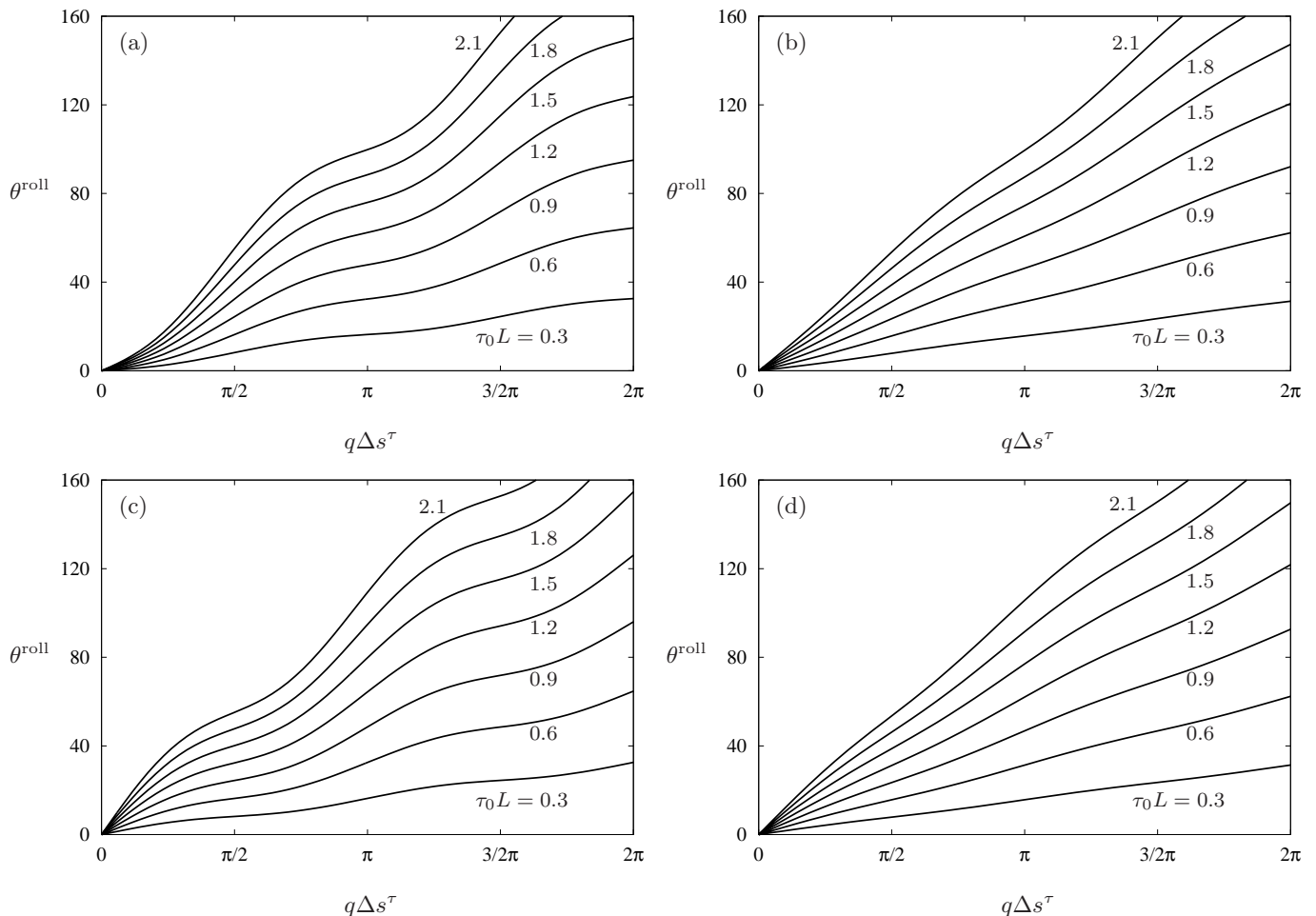


FIG. 12. Roll reorientation angle θ^{roll} vs normalized torsional mode length $q\Delta s^\tau$. Panels (a) and (c) show results for *C*-shaped gait ($qL = 5.5$), and panels (b) and (d) show results for *W*-shaped ($qL = 9$) gait. Normalized magnitude of body torsion $\tau_0 L$ as labeled. The initial mode-switching point occurs when the curvature at the head position is at a maximum [panels (a) and (b)] and at a minimum [panels (c) and (d)].

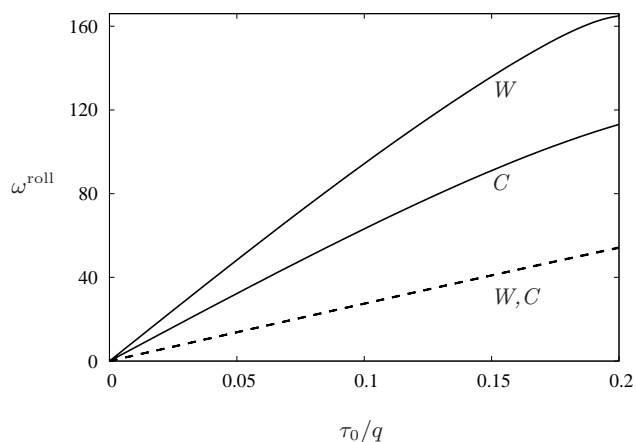


FIG. 13. Roll rotation rate per undulation period ω^{roll} (in degrees) vs normalized magnitude of body torsion τ_0/q for nematode performing one-mode rolls for swimming (solid lines) and burrowing (dashed lines). Results correspond to $A/q = 1$ for *C*-shaped and *W*-shaped locomotive gaits, as labeled.

one to two periods of motion to roll by 90° , and rolls by 90° in less than one period are not unusual. According to the results shown in Figs. 11 and 12, a 90° roll corresponds to the body torsion of $\tau_0 L \approx 1$ for the roll mode length ranging from half to one undulation period. Shorter modes require larger torsion (see, e.g. Video S4 in ESM).

3.2.1. Hydrodynamic enhancement in swimming rolls

To compare the swimming roll rotation rate ω^{roll} shown in Fig. 11 with the corresponding purely geometrical no-slip result (Fig. 4), the swimming and no-slip simulation data are replotted in Fig. 13 using the same scaling of the torsion τ_0/q for both data sets. The results indicate that hydrodynamic forces in swimming can enhance the rotation rate by a factor ranging from approximately two (*C*-shaped gait) to even three (*W*-shaped gait). While this hydrodynamic enhancement may seem

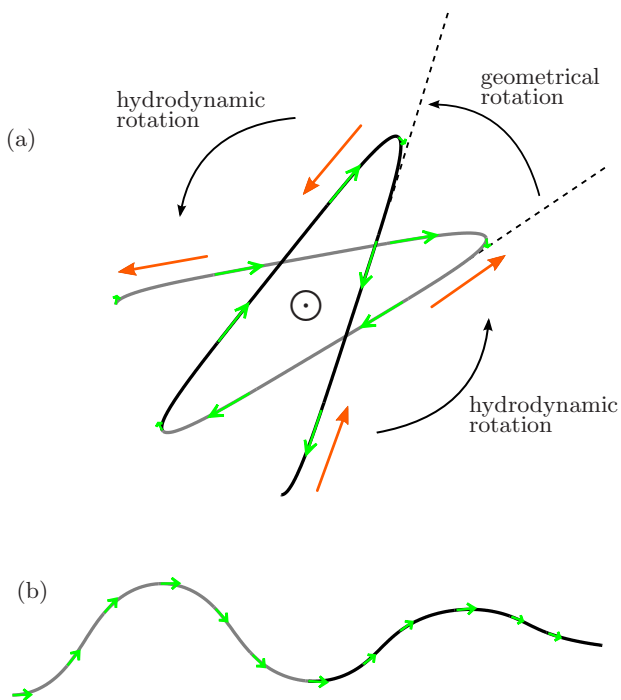


FIG. 14. (a) Front and (b) side views of a trajectory reproduced from sinusoidal curvature with $A/q = 1$ and constant torsion $\tau/q = 0.15$. The first period of undulation is shown in gray and the second in black. The symbol \odot denotes the direction of propagation of the curve (out of the page) and the green arrows represent the unit tangent vector \hat{t} (in the direction of nematode motion). In the presence of a fluid, the nematode moving along the curve experiences hydrodynamic resistance force (represented by orange arrows) oriented in the same direction as the geometrical rotation of the undulation plane.

surprising, its origin can be explained by a careful examination of hydrodynamic forces acting on a nematode performing a torsional roll in the absence of sidewise slip.

The projection of a torsional no-slip trail onto the plane normal to the overall direction of motion is depicted in Fig. 14. The graph shows that the plane of undulations gradually rotates anticlockwise, whereas the nematode moves clockwise around the axis of the trajectory. In fluids, this clockwise motion produces the oppositely oriented hydrodynamic resistance, which causes hydrodynamically induced nematode rotation in the anticlockwise direction. Since the geometrical and hydrodynamic contributions to ω^{roll} have the same sign, they add up, resulting in the enhanced reorientation.

We believe that swimming *C. elegans* use the above hydrodynamic enhancement mechanism in the observed rapid roll maneuvers (see Video S3 in ESM). Our numerical simulations presented in Video S4 in ESM reproduce this behavior.

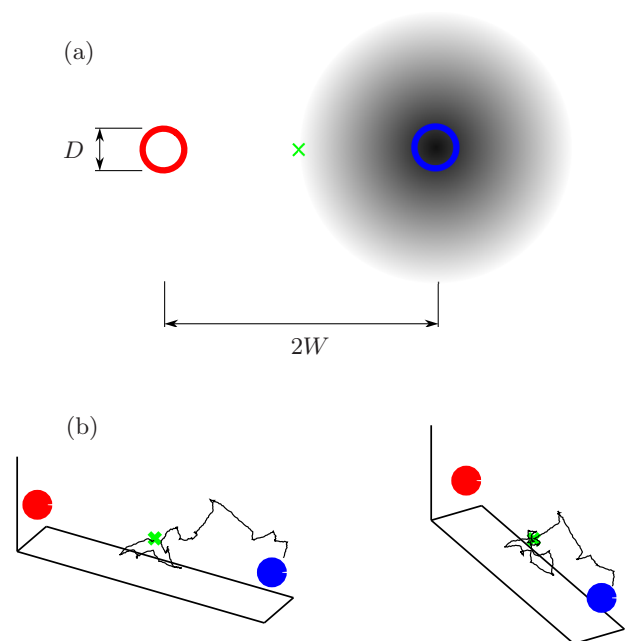


FIG. 15. (Colour online) (a) Top view of the simulated chemotaxis assay in 3D. Nematodes are initialized with a random orientation at the green symbol \times located midway between the position of a Gaussian chemoattractant concentration peak (right) and a spherical control region represented by the left red circle. The right blue circle represents a spherical test region. (b) Two views of a simulated path followed by a chemotaxing *C. elegans* in a 3D fluid.

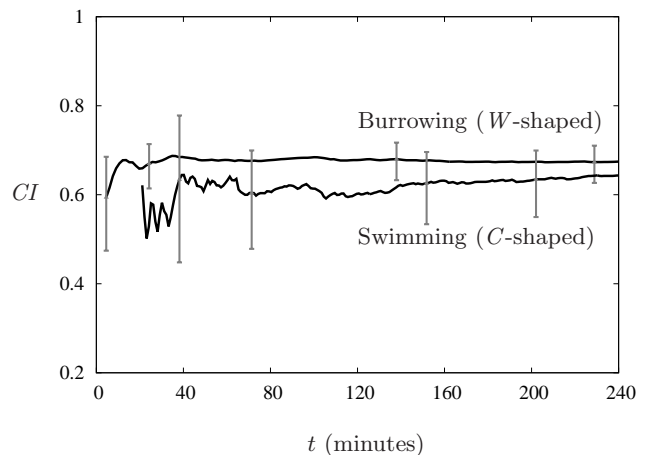


FIG. 16. Chemotaxis index CI vs time for burrowing and swimming nematodes in 3D. The sensing parameters for the burrowing and the swimming cases are the same, but the undulation frequency of the swimmer is four times larger than the undulation frequency of the burrower.

4. APPLICATION TO CHEMOTAXIS

According to the locomotion model developed in Secs. 2 and 3, *C. elegans* navigates 3D environments by combining forward motion, planar turns, and torsional rolls

Parameter	Name	Value
α'_s	Chemoattractant sensitivity parameter	5 s/mm
r_s^0	Turn initiation rate	10 turns/min
r_s^H	Upper turn-rate saturation limit	15 turns/min
r_s^L	Lower turn-rate saturation limit	5 turns/min
r_τ^0	Roll initiation rate	37 rolls/min
ϵ	Memory time constant	1.6 s^{-1}
A_1/q	Forward mode normalized amplitude	1
f_b	Burrowing gait frequency	0.44 s^{-1}
f_s	Swimming gait frequency	1.75 s^{-1}
$q_b L$	Burrowing gait normalized wavevector	9
$q_s L$	Swimming gait normalized wavevector	5.5
L	Worm length	1 mm

TABLE I. System parameters for 3D simulations of chemotaxis of burrowing and swimming *C. elegans*. The chemoattractant sensitivity parameter $\alpha'_s = \alpha_s / \nabla C|_{r=\sigma}$ is normalized by the maximum chemical concentration gradient located at $r = \sigma$. The memory time constant ϵ corresponds to an approximately 5 s half-decay response time of sensory neurons to the step increase of chemoattractant concentration [34].

(see Videos S1 and S5 in ESM for simulations of burrowing and swimming behavior). Here we show that by modulating the rate of the above elementary maneuvers in response to a chemoattractant concentration variation, *C. elegans* can efficiently chemotax in 3D.

It has been demonstrated that in 2D environments *C. elegans* employs two chemotaxis mechanisms: klinotaxis (gradual turn) where the nematode actively reorients itself towards the concentration gradient direction [35], and klinokinesis (biased random walk), where it adjusts time intervals of motion in favorable and unfavorable directions to achieve a net displacement towards the higher concentration [36].

While we expect both strategies to be effective in 3D, in the present paper we focus on the biased random walk (BRW) mechanism. A more comprehensive study of nematode chemotaxis in complex environment will be described elsewhere.

4.1. Chemical sensing model

A moving *C. elegans* assesses the spatial gradients of the chemoattractant concentration by monitoring its time variation $C(t)$ at the current position of chemical receptors (located in the nematode head segment) [37]. To model this process we use an approach that has been successfully applied to describe bacterial chemotaxis [38].

Accordingly, we assume that the rate of turns is modulated by the chemical signal

$$Q(t) = \int_0^t C(t-t')M(t')dt', \quad (11)$$

where $M(t)$ is the memory function that describes the response of sensory neurons to chemoattractant. Assum-

ing that the nematode responds to changes of the concentration of chemoattractant but not to the absolute concentration value [37], we impose the ideal adaptation condition [38]

$$\int_0^\infty M(t)dt = 0. \quad (12)$$

We also assume the normalization

$$\int_0^\infty tM(t)dt = 1. \quad (13)$$

In our numerical calculation we use the memory function defined by the expression

$$M(t) = \epsilon^2 e^{\epsilon t} \left[(\epsilon t) - \frac{1}{2}(\epsilon t)^2 \right], \quad (14)$$

where ϵ^{-1} is the decay time [38]. The memory function (14) is positive for $0 < t < \epsilon^{-1}$ and negative for $t > \epsilon^{-1}$; the positive and negative regions have equal integrals. The convolution integral (11) filters out short-time fluctuations of the chemoattractant concentration and provides information whether the concentration is increasing ($Q > 0$) or decreasing ($Q < 0$) on the timescale ϵ^{-1} .

4.2. Biased random walk

A nematode performing BRW generates a trajectory drift towards a peak of chemoattractant concentration by controlling the frequency of random turns in response to sensory signals. Namely, to achieve longer intervals of motion towards the peak, the turn rate is reduced (increased) when the animal moves towards (away from) the peak. In our chemotaxis model, the chemical signal Q controls the frequency of elementary three-mode turns.

The nematode burrows or swims using the default harmonic-curvature locomotion mode with $A/q \approx 1$, and switches randomly to a turning mode at a turn initiation rate $r_s(t)$, which depends on the chemotaxis signal (11). The nematode also performs roll maneuvers initiated at a rate $r_\tau(t)$.

To mimic the experimentally observed sigmoidal character of the turn response to the chemoattractant concentration variation [36], we assume that the turn initiation rate r_s has a linear-response region and a saturation cut-off,

$$r_s(t) = \begin{cases} r_s^L; & f(Q) \leq r_s^L \\ f(Q); & r_s^L < f(Q) < r_s^H, \\ r_s^H; & r_s^H \leq f(Q) \end{cases} \quad (15)$$

where

$$f(Q) = r_s^0 [1 - \alpha_s Q(t)]. \quad (16)$$

Here r_s^0 is the turn rate in the absence of chemoattractant, α_s is a chemoattractant sensitivity parameter, and r_s^H and r_s^L are the saturation limits. Since there are no experimental data regarding the effect of chemoattractant on roll maneuvers, we assume that the roll initiation frequency is constant and independent of chemical sensing,

$$r_\tau(t) = r_\tau^0. \quad (17)$$

In Sec. 4.4 we show that assumptions (15) and (17) are sufficient to produce efficient 3D chemotaxis.

4.3. The geometry of simulated chemotaxis assay

In our 3D numerical simulations of chemotaxis of burrowing and swimming nematodes [see Fig. 15(a)], the simulated worms are placed at a designated starting point at the edge of a Gaussian chemoattractant concentration distribution. The chemotaxis efficiency is determined by comparing the number of nematodes that reach a spherical test region at the chemoattractant concentration peak with the number of those that reach a symmetrically placed control region in the low-concentration domain. Our 3D arrangement mimics a typical experimental setup for investigating 2D chemotaxis on agar surface [39, 40].

The chemotaxis efficiency is quantified using the chemotaxis index

$$CI(t) = \frac{n_t(t) - n_c(t)}{n_t(t) + n_c(t)}, \quad (18)$$

where $n_t(t)$ and $n_c(t)$ denote the number of nematodes that reached the test and control regions, respectively, during the simulation interval $[0, t]$. The simulation of a nematode trajectory is terminated when the nematode enters either the test or control region (in 2D laboratory experiments these regions usually contain anesthetic to

immobilize the nematodes [40]). A sample trajectory of a swimming *C. elegans* reaching the test region is shown in Fig. 15(b).

In our simulations we consider a system with the following parameters. The spatial concentration of chemoattractant is given by a 3D Gaussian distribution

$$C \sim \exp(-r^2/2\sigma^2) \quad (19)$$

with the peak position at a distance $W = 36L$ from the starting point and the width $\sigma = 0.4W$. The diameter of the test and control regions is $D = 10L$. For the worm length $L = 1$ mm, the starting point is thus at a distance 3.6 cm from the chemoattractant concentration maximum, and the test and control regions have a 1 cm diameter (similar to the geometry of 2D experiments in a Petri dish).

4.4. Simulation results

We have performed simulations for two cases: (a) burrowing W -shaped nematodes (no transverse slip) and (b) swimming C -shaped nematodes. The nematode gait parameters and parameters of the chemotaxis model are listed in Table I (see Sec. 6.2 for more details). The gait parameter values are based on observations of crawling and swimming *C. elegans*. We use the same chemosensation and turn-rate parameters in the burrowing and swimming simulations to isolate the effect of the locomotion mechanics on the chemotaxis efficiency.

Chemotaxis index (18), shown in Fig. 16, is significantly greater than zero, indicating a clear trajectory bias towards the chemoattractant concentration peak. At long times the value of CI for both burrowing and swimming is approximately the same. However, the burrowing nematodes are able to reach the chemoattractant peak more quickly, due to the higher burrowing velocity (twice the swimming velocity for the gait parameters considered).

The chemotaxis index for burrowing and swimming nematodes is similar due to two compensating effects: (a) for swimming nematodes the chemical signal (11) is weaker because, as a result of their lower velocity, swimming worms detect a smaller time variation of chemoattractant concentration; while (b) the number of turns per unit trajectory length is larger for swimming nematodes because of their lower velocity. More turns implies a stronger bias towards chemoattractant, which compensates for a weaker chemical signal.

We expect that similar compensating factors occur in other environments as well. Thus, the nematode may achieve efficient chemotaxis without adjusting turn-rate control parameters in response to a variation in mechanical properties of the medium in which it moves; a more complex control system that relies on mechanical feedback is unnecessary.

The values of the 2D and 3D chemotaxis index do not differ either, but in 3D many more nematodes escape

without reaching either the test or control region; this effect should be taken into account in design of a testing platform for future 3D chemotaxis experiments.

5. SUMMARY AND DISCUSSION

To provide mathematical tools for analysis of 3D nematode maneuvers, we have developed a gait model that combines piecewise-harmonic-curvature (PHC) and piecewise-constant-torsion (PCT) body-shape assumptions. We have demonstrated that nematode reorientation in an arbitrary direction can be achieved by a mix of 2D turns (driven by changes of curvature-wave parameters) and 3D roll maneuvers (associated with nonzero body torsion).

We have applied our model to investigate 3D motion of nematodes burrowing in gels and swimming in Newtonian fluids. We examined the effectiveness of the turns and rolls; our modeling of torsional roll maneuvers reveals a strong enhancement of the roll-rotation rate due to hydrodynamic forces. This hydrodynamic effect may explain the observed rapid reorientation of the undulation plane of swimming *C. elegans* (see video S3 in ESM).

We have used our gait representation to study nematode chemotaxis in gels and fluids. We have shown that the nematode does not need to adjust its sensory-motor apparatus to effectively respond to chemical stimuli in environments with different mechanical properties. Chemotaxis of *C. elegans* in 3D environments was experimentally demonstrated [20, 41], but, to our knowledge, the formulation presented here is the first quantitative analysis that takes into account the gait geometry and swimming mechanics.

By supplying an analytical description of elementary body movements, our PHC/PCT gait model is applicable to analyze nematode behavior in 3D complex media, including inhomogeneous materials and non-Newtonian fluids. We expect that our results may also shed light on other subtle aspects of neuromuscular control of 3D locomotion of *C. elegans*.

Body movements of *C. elegans* are actuated by coordinated action of four quadrants of body muscles, which are arranged into double rows that span the entire body length [42]. While this muscle anatomy is compatible with 3D body actuation, it is less clear how the neural system can activate differential muscle contractions needed to generate 3D body deformations out of the dorsoventral undulation plane.

The head and neck body muscles are innervated by the nerve ring motor neurons, which synapse onto cells in individual quadrants (and thus are capable to actuate each quadrant individually). In contrast, the remaining body muscles are innervated only by the ventral-cord motor neurons, which synapse onto muscles of either two ventral or two dorsal quadrants, consistent with 2D actuation [42–44]. Based on this topology of neural connections, it is generally assumed that only the head and

neck segments can perform 3D motion.

However, the stereoscopic experiments by Kwon *et al.* [18] clearly show that burrowing nematodes can adopt a variety of 3D postures, in which the entire body undergoes out-of-plane deformations. In the swimming case the evidence is less conclusive because stereoscopic images are not available. Nonetheless, two-dimensional images, such as the one shown in Fig. 9, agree qualitatively with our 3D body posture model.

Our hydrodynamic calculations of the roll dynamics further support a conclusion that the entire nematode body participates in generating the roll motion. In particular, we find that torsional wave propagating throughout the entire body length can produce a 90° roll in less than one undulation period. In contrast, a stroke in which only the head and neck segments are displaced out of the undulation plane produces weaker rolls than the ones observed in our experiments (see the results of our additional simulations in Fig. S2 in ESM).

We hypothesize that the generation of a nonzero torsion in the posterior part of the nematode body involves a 3D proprioceptive feedback, which enables propagation of the torsional wave to the body region innervated only by the ventral-cord motor neurons. The existence of 2D proprioceptive feedback in *C. elegans* and its important role in generation of a planar undulation wave have been demonstrated [4]. We thus conjecture that *C. elegans* may employ 3D proprioception to generate well controlled out-of-plane body movements. (An alternative hypothesis would be that the worm may control its 3D body movements using direct communication between muscle cells via gap junctions.)

Current evidence is not sufficient to rule out a passive, purely mechanical origin of propagation of 3D deformations along a portion of the nematode body outside the head and neck regions. In particular, the body shapes observed during burrowing [18] can, in principle, be generated by 3D actuation of the head and neck muscles, with the rest of the body passively sliding along the tunnel carved by the nematode head. Such motion, however, would be inefficient.

According to Wen *et al.* [4], “[t]he cellular economy of the *C. elegans* wiring diagram implies that individual neurons may have high levels of complexity” (for example, B-type motor neurons are able to transduce proprioception). We conclude that it is thus conceivable that functional complexity on a single-neuron level allows symmetrically connected neurons to produce differential muscle excitation.

Nature created a four-quadrant muscle arrangement that is anatomically capable of generating 3D body deformations. Therefore, our question is: why should there not be a compatible neuromuscular-control system that would allow the nematode to take advantage of this (existing) muscle structure? Further analyses of 3D locomotion of *C. elegans* will help determine if such a control system exists.

6. METHODS

6.1. Imaging

Wild type *C. elegans* was used to record the 3D swimming in our experiments. Worms were cultured in NGM plate (Nematode Growth Medium) seeded with bacteria *E. coli* OP50 at 20°C. A liquid pool was created for swimming assay by adding 5–7 mL of M9 buffer into a 60 mm Petri dish. The pool height was approximately 2 mm. The surface of the Petri dish was treated with 5% Pluronic F127 for 5 min before adding M9 buffer. Individual young adults were manually transferred into a liquid pool of M9 buffer using a worm pick. Swimming episodes were recorded at 5 frames per second using an SVSI camera and Zeiss stemi 2000-C stereo microscope imaging system at 1.6X magnification with a pixel resolution of 0.21 pixels/ μm . All imaging was carried out in a food-free environment at 20°C.

6.2. Chemotaxis simulation details

In our simulations, the planar turns and rolls are initiated randomly at the rates r_s and r_τ , provided that a reorientation maneuver of the same kind is not already taking place. The turns and rolls are performed independently.

The default gait parameters (used between reorientation maneuvers) have fixed values listed in Table I. The parameters of the turn and roll modes are chosen randomly from Gaussian distributions. The average parameter values (indicated by overbar) and standard deviations

σ are: normalized turning-mode amplitude $\overline{A_2}/q = 1.67$ and $\sigma_{A_2/q} = 0.28$; turning-mode length $\overline{\Delta s^c}/L = 0.5$ and $\sigma_{\Delta s^c/L} = 0.167$; normalized torsion $\overline{\tau_0}L = 2$ and $\sigma_{\tau_0L} = 1$; and torsional-mode length $\overline{\Delta s^\tau}/L = 0.5$ and $\sigma_{\Delta s^\tau/L} = 0.1$. The parameter distributions are the same for burrowing and swimming.

The turning rates listed in Table I correspond to the directional persistence length of burrowing trajectories $l_p \approx 12L$ (which is of the same order as the persistence length observed in crawling). We define the persistence length l_p as half-decay length of the directional correlation function. The rate of roll maneuvers was chosen such that on average the worm spends half the time in a torsionless state.

Authors' contributions. AB wrote the manuscript, developed locomotion and hydrodynamic codes, and performed locomotion and chemotaxis simulations. AP provided chemotaxis formulations and codes and performed some chemotaxis simulations. MR provided experimental images of the worm. SAV provided experimental images and helped develop conceptual framework and draft the manuscript. JB conceived the study and wrote the manuscript.

Funding. AB would like to acknowledge financial support from NSF Grant CBET 1059745 and TTU Doctoral Dissertation Completion Fellowship. JB was partially supported from NSF Grant CBET 1603627. SAV and MR acknowledge partial support from Grants NIH 1R21AG050503-01 and NASA NNX15AL16G.

Acknowledgments. We would like to thank our visiting undergraduate researcher, Jose Montoya, for his help in developing chemotaxis codes and acknowledge Dr. Szewczyk and Dr. Driscoll for useful discussions.

Competing interests. We have no competing interests.

-
- [1] A. Ghanbari, V. Nock, S. Johari, R. Blaikie, X. Chen, and W. Wang, “A micropillar-based on-chip system for continuous force measurement of *C. elegans*,” *J. Micromech. Microeng.* **22**, 095009 (2012).
- [2] S. Johari, V. Nock, M. M. Alkaiji, and W. Wang, “On-chip analysis of *C. elegans* muscular forces and locomotion patterns in microstructured environments,” *Lab. Chip.* **13**, 1699–1707 (2013).
- [3] T. Etheridge, M. Rahman, C. J. Gaffney, D. Shaw, F. Shephard, J. Magudia, D. E. Solomon, T. Milne, J. Blawdziewicz, D. Constantin-Teodosiu, P. L. Greenhaff, S. A. Vanapalli, and N. J. Szewczyk, “The integrin-adhesion is required to maintain muscle structure, mitochondrial ATP production, and movement forces in *Caenorhabditis elegans*,” *FASEB J* **29**, 1235–1246 (2015).
- [4] Q. Wen, M. D. Po, E. Hulme, S. Chen, X. Liu, S. W. Kwok, M. Gershow, A. M. Leifer, V. Butler, C. Fang-Yen, T. Kawano, W. R. Schafer, G. Whitesides, M. Wyart, D. B. Chklovskii, M. Zhen, and A. D. T. Samuel, “Proprioceptive Coupling within Motor Neurons Drives *C. elegans* Forward Locomotion,” *Neuron* **76**, 750–761 (2012).
- [5] J. N. Stirman, M. M. Crane, S. J. Husson, S. Wabnick, C. Schultheis, A. Gottschalk, and H. Lu, “Real-time multimodal optical control of neurons and muscles in freely behaving *Caenorhabditis elegans*,” *Nat. Methods.* **8**, 153–159 (2011).
- [6] J. M. Gray, J. J. Hill, and C. I. Bargmann, “A circuit for navigation in *Caenorhabditis elegans*,” *Proc. Natl. Acad. Sci. U.S.A.* **102**, 3184–3191 (2005).
- [7] A. Kocabas, C.-H. Shen, Z. V. Guo, and S. Ramanathan, “Controlling interneuron activity in *Caenorhabditis elegans* to evoke chemotactic behaviour,” *Nature* **490**, 273–277 (2012).
- [8] J. Sznitman, P. K. Purohit, P. Krajacic, T. Lamitina, and P. E. Arratia, “Material properties of *Caenorhabditis elegans* swimming at low Reynolds number,” *Biophys. J.* **98**, 617–626 (2010).
- [9] A. E. X. Brown, E. I. Yemini, L. J. Grundy, T. Jucikas, and William R. Schafer, “A dictionary of behavioral motifs reveals clusters of genes affecting *Caenorhabditis elegans* locomotion,” *Proc. Natl. Acad. Sci. U.S.A.* **110**, 791–796 (2013).
- [10] C. Restif, C. Ibanez-Ventoso, M. M. Vora, S. Guo, D. Metaxas, and M. Driscoll, “CeleST: Computer Vision Software for Quantitative Analysis of *C. elegans* Swim Behavior Reveals Novel Features of Locomotion,” *PLoS*

- Comput. Biol. **10**, 1–12 (2014).
- [11] M. Artal-Sanz, L. de Jong, and N. Tavernarakis, “*Caenorhabditis elegans*: A versatile platform for drug discovery,” J. Biotechnol. **8**, 1405–1418 (2011).
- [12] D. T. Omura, D. A. Clark, A. D. T. Samuel, and H. R. Horvitz, “Dopamine signaling is essential for precise rates of locomotion by *C. elegans*,” PLoS ONE **7**, e38649 (2012).
- [13] N. Cohen and J. H. Boyle, “Swimming at low Reynolds number: a beginners guide to undulatory locomotion,” Contemp. Phys. **51**, 103–123 (2010).
- [14] C. Fang-Yen, M. Wyart, J. Xie, R. Kawai, T. Kodger, S. Chen, Q. Wen, and A. D. T. Samuel, “Biomechanical analysis of gait adaptation in the nematode *Caenorhabditis elegans*,” Proc. Natl. Acad. Sci. U.S.A. **107**, 20323–8 (2010).
- [15] J. Sznitman, X. Shen, P. K. Purohit, and P. E. Arratia, “The effects of fluid viscosity on the kinematics and material properties of *C. elegans* swimming at low Reynolds number,” Exp. Mech. **50**, 1303–1311 (2010).
- [16] V. Padmanabhan, Z. S. Khan, D. E. Solomon, A. Armstrong, K. P. Rumbaugh, S. A. Vanapalli, and J. Blawdziewicz, “Locomotion of *C. elegans*: a piecewise-harmonic curvature representation of nematode behavior,” PLoS ONE **7**, e40121 (2012).
- [17] G. J. Stephens, B. Johnson-Kerner, W. Bialek, and W. S. Ryu, “Dimensionality and dynamics in the Behavior of *C. elegans*,” PLoS Comput. Biol. **4**, e1000028 (2008).
- [18] N. Kwon, J. Pyo, S. Lee, and J. Je, “3-D Worm Tracker for Freely Moving *C. elegans*,” PLoS ONE **8**, e57484 (2013).
- [19] N. Kwon, A. B. Hwang, Y.-J. You, S.-J. V. Lee, and J. H. Je, “Dissection of *C. elegans* behavioral genetics in 3-D environments,” Sci. Rep. **5**, 09564 (2015).
- [20] C. Beron, A. G. Vidal-Gadea, J. Cohn, A. Parikh, G. Hwang, and J. T. Pierce-Shimomura, “The burrowing behavior of the nematode *Caenorhabditis elegans*: a new assay for the study of neuromuscular disorders,” G2B **14**, 357–368 (2015).
- [21] X. Deng and J. Xu, “A 3d undulatory locomotion model inspired by *C. elegans* through DNN approach,” Neurocomputing **131**, 248–264 (2014).
- [22] B. Delmotte, E. Climent, and F. Plouraboue, “A general formulation of bead models applied to flexible fibers and active filaments at low Reynolds number,” J. Comput. Phys. **286**, 14–37 (2015).
- [23] J. Sznitman, X. Shen, R. Sznitman, and P. E. Arratia, “Propulsive force measurements and flow behavior of undulatory swimmers at low Reynolds number,” Phys. Fluids **22**, 12901 (2010).
- [24] S. J. Husson, W. S. Costa, C. Schmitt, and A. Gottschalk, “Keeping track of worm trackers (September 10, 2012),” *The C. elegans Research Community*, WormBook, doi/10.1895/wormbook.1.156.1, <http://www.wormbook.org>.
- [25] R. S. Berman, O. Kenneth, J. Sznitman, and A. M. Leshansky, “Undulatory locomotion of finite filaments: lessons from *C. elegans*,” New J. Phys. **15**, 075022 (2013).
- [26] A. Bilbao, E. Wajnryb, S. A. Vanapalli, and J. Blawdziewicz, “Nematode Locomotion in Unconfined and Confined Fluids,” Phys. Fluids. **25**, 081902 (2013).
- [27] D. Kim, S. Park, L. Mahadevan, and J. H. Shin, “The shallow turn of a worm,” J. Exp. Biol. **214**, 1554–1559 (2011).
- [28] J. Stoker, *Differential Geometry* (John Wiley and Sons, New York, 1969).
- [29] W. Voorhies, J. Fuchs, and S. Thomas, “The longevity of *Caenorhabditis elegans* in soil,” Biol. Lett. , 247–249 (2005).
- [30] L. Frezal and M. Felix, “The natural history of model organisms: *C. elegans* outside the petri dish,” eLife **4**, e05849 (2015).
- [31] H. Lee, M.-K. Choi, D. Lee, H.-S. Kim, H. Hwang, H. Kim, S. Park, Y.-K. Paik, and J. Lee, “Nictation, a dispersal behavior of the nematode *Caenorhabditis elegans*, is regulated by IL2 neurons,” Nature Neurosci **15**, 107–112 (2012).
- [32] E. Wajnryb, K. A. Mizerski, P. J. Zuk, and P. Szymczak, “Generalization of the Rotne-Prager-Yamakawa mobility and shear disturbance tensors,” J. Fluid Mech. **731**, R3 (2013).
- [33] B. Cichocki, B. U. Felderhof, K. Hinsen, E. Wajnryb, and J. Blawdziewicz, “Friction and mobility of many spheres in Stokes flow,” J. Chem. Phys. **100**, 3780–3790 (1994).
- [34] H. Suzuki, T. R. Thiele, S. Faumont, M. Ezcurra, S. R. Lockery, and W. R. Schafer, “Functional asymmetry in *Caenorhabditis elegans* taste neurons and its computational role in chemotaxis,” Nature **454**, 114–118 (2008).
- [35] Y. Iino and K. Yoshida, “Parallel Use of Two Behavioral Mechanisms for Chemotaxis in *Caenorhabditis elegans*,” J. Neurosci. **29**, 5370–5380 (2009).
- [36] J. T. Pierce-Shimomura, T. M. Morse, and S. R. Lockery, “The fundamental role of pirouettes in *Caenorhabditis elegans* chemotaxis,” J. Neurosci. **19**, 9557–9569 (1999).
- [37] S. R. Lockery, “The computational worm: spatial orientation and its neuronal basis in *C. elegans*,” Curr Opin Neurobiol **21**, 782–790 (2011).
- [38] A. Celani and M. Vergassola, “Bacterial strategies for chemotaxis response,” Proc. Natl. Acad. Sci. U.S.A. **107**, 1391–1396 (2010).
- [39] C. I. Bargmann and H. R. Horvitz, “Chemosensory neurons with overlapping functions direct chemotaxis to multiple chemicals in *c. elegans*,” Neuron. **7**, 729–742 (1991).
- [40] A. Nishino, F. Sato, K. Ito, and T. Matsuura, “Extension of the established period of diacetyl adaptation by oxygen intermediates in the nematode *Caenorhabditis elegans*,” Comp. Biochem. Physiol. A: Physiol. **184**, 156–162 (2015).
- [41] J. T. Pierce-Shimomura, B. L. Chen, J. J. Mun, R. Ho, R. Sarkis, and S. L. McIntire, “Genetic analysis of crawling and swimming locomotory patterns in *C. elegans*,” Proc. Natl. Acad. Sci. U.S.A. **105**, 20982–20987 (2008).
- [42] Z. F. Altun and D. H. Hall, “Muscle system, somatic muscle.” In WormAtlas (2009).
- [43] J. G. White, E. Southgate, J. N. Thomson, and S. Brenner, “The structure of the nervous system of the nematode *Caenorhabditis elegans*,” Philos. Trans. R. Soc. London, Ser. B **314**, 1–340 (1986).
- [44] D. L. Riddle, T. Blumenthal, B. J. Meyer, and J. R. Priess, *C. elegans II. 2nd edition*. (Spring Harbor, 1997) section I, Introduction: the Neural Circuit For Locomotion.